Quantum annealing for hard 2-satisfiability problems: Distribution and scaling of minimum energy gap and success probability

Vrinda Mehta,[1,2] Fengping Jin,[1] Hans De Raedt,[1,3] and Kristel Michielsen[1,2,4,*]

[1]*Institute for Advanced Simulation, Jülich Supercomputing Centre, Forschungszentrum Jülich, 52425 Jülich, Germany*

[2]*RWTH Aachen University, 52056 Aachen, Germany*

[3]*Zernike Institute for Advanced Materials, University of Groningen, Nijenborgh 4, 9747 AG Groningen, Netherlands*

[4]*Center for Simulation and Data Science, Jülich Aachen Research Alliance, 52425 Jülich, Germany*

(Received 3 February 2022; revised 5 May 2022; accepted 13 May 2022; published 3 June 2022)

In recent years, quantum annealing has gained the status of being a promising candidate for solving various optimization problems. Using a set of hard 2-satisfiability (2-SAT) problems, consisting of problems of up to 18 variables, we analyze the scaling complexity of the quantum annealing algorithm and study the distributions of the minimum energy gap and the success probability. We extend the analysis of the standard quantum annealing Hamiltonian by introducing an additional term, the trigger Hamiltonian, which can be of two types: ferromagnetic and antiferromagnetic. We use these trigger Hamiltonians to study their influence on the success probability for solving the selected 2-SAT problems. We find that although the scaling of the runtime is exponential for the standard and modified quantum annealing Hamiltonians, the scaling constant in the case of adding the trigger Hamiltonians can be significantly smaller. Furthermore, certain choices for the trigger Hamiltonian and annealing times can result in a better scaling than that for simulated annealing. Finally, we also use the quantum annealers of D-Wave Systems Inc. to study their performance in solving the 2-SAT problems and compare it with the simulation results.

DOI: 10.1103/PhysRevA.105.062406

I. INTRODUCTION

Quantum annealing is a metaheuristic for solving combinatorial optimization problems, which requires mapping the problem to the Ising Hamiltonian. The ground state of this so-called problem Hamiltonian encodes the solution to the optimization problem, and therefore the task of finding the solution to the optimization problem is equivalent to finding the ground state of the problem Hamiltonian. Similar to simulated annealing [1], where the search for the ground state is assisted by adding thermal fluctuations, quantum annealing makes use of quantum fluctuations so that quantum tunneling can facilitate the search for the lowest-energy configuration [2–4].

The idea of employing adiabatic quantum annealing to realize a quantum computer devoted to solving optimization problems emerged in the early 2000s [5,6]. However, the notion of quantum annealing has a wider scope than adiabatic quantum computing as it also allows for nonadiabatic transitions during the evolution [7–9]. A similar algorithm that has been developed for the gate-based model of quantum computing is the quantum approximate optimization algorithm [10–14].

Since its conception, there has been extensive research to evaluate the efficiency of quantum annealing in solving optimization problems [15–25]. Moreover, the availability of commercial quantum annealers of D-Wave, which offers annealing systems with more than 5000 qubits [26], has given the impetus for research in this direction [14,27–39]. Much of the work has focused on investigating whether quantum annealing can deliver a speedup over the existing classical algorithms [20,33,40]. A related area of interest is to assess the performance of quantum annealing by studying the scaling of the computation time required to solve the optimization problem as a function of the problem size and comparing it to the scaling of certain chosen classical algorithms [31,33,40–45].

In this work we numerically investigate the scaling complexity of quantum annealing for solving 13 sets of 2-satisfiability (2-SAT) problems, with the size of the problems varying from 6 to 18 variables [46]. These problems have a known ground state and have been specially designed to be hard to solve using simulated annealing [43,46]. Therefore, such an analysis allows us to gauge the suitability of quantum annealing for solving them.

In the case of adiabatic quantum annealing, the minimum energy gap between the ground state and the first excited state of the Hamiltonian is a pivotal quantity for determining the computation time required to obtain the solution for the optimization problem [47]. Hence, we look at the scaling of the minimum energy gaps to understand how the resources required to solve these problems using quantum annealing grow as the problem size increases. For a comparison with the predictions of the adiabatic theorem, we also determine the scaling of the time to solution $\mathcal{T}_{99}$, which is the runtime required to obtain the ground state of the problem Hamiltonian at least once, in multiple runs of the algorithm, with 99% certainty.

*Corresponding author: k.michielsen@fz-juelich.de

Next, to examine how modifications to the standard algorithm affect these scalings, we add a third term [9,22,48–52], the trigger Hamiltonian, to the standard algorithm for quantum annealing, which vanishes at the beginning and end of the annealing process. Furthermore, the trigger Hamiltonian can be of two types, the ferromagnetic trigger Hamiltonian and the antiferromagnetic trigger Hamiltonian [9,52]. Previous findings have indicated that while the inclusion of the ferromagnetic trigger Hamiltonian mostly enlarges the minimum energy gaps, therefore promoting the chances of an adiabatic evolution, adding the antiferromagnetic trigger Hamiltonian can either increase or decrease the size of the minimum energy gaps [9,52]. In addition, it can also modify the energy spectrum of the quantum annealing Hamiltonian significantly, for example, by increasing the number of anticrossings between the ground state and the first excited state of the Hamiltonian or by altering the shape of the anticrossing, giving way to some interesting nonadiabatic mechanisms that control the evolution of the state of the system [52]. Thus, a study of the scaling of the minimum energy gaps and $\mathcal{T}_{99}$ with the addition of the trigger Hamiltonians facilitates a direct comparison between the adiabatic quantum annealing and the quantum annealing algorithm allowing for nonadiabatic mechanisms.

Finally, we also use the solvers offered by D-Wave to study the scaling of the $\mathcal{T}_{99}$ on these systems. Although susceptible to noise and temperature effects, these systems provide the hardware for the largest quantum annealer. A comparison of the results obtained with these systems with the simulation results can give insight into how close these systems are to an ideal quantum annealer, as well as the dominant effects playing a role during the evolution of the state of the system.

We analyze the distribution of the minimum energy gap between the ground state and the first excited state of the quantum annealing Hamiltonian, and the success probability, as well as the scaling behavior of the minimum energy gap and the $\mathcal{T}_{99}$. We obtain three distinct distributions for the minimum energy gaps. In the adiabatic limit, these distributions can be extrapolated to the distribution of the success probability using the Landau-Zener theory. For certain distributions of the minimum energy gaps, the resulting distribution for the success probability is predicted to be constant. The simulation results for the success probability distribution are found to be of three kinds: bimodal, unimodal, and constant. Interestingly, the corresponding results obtained with the D-Wave annealers also show these three distributions. The scaling of the minimum energy gaps and the $\mathcal{T}_{99}$ in the adiabatic regime is found to be exponential in the asymptotic limit. Furthermore, we find that in the adiabatic limit, the standard quantum annealing Hamiltonian results in a worse scaling of the $\mathcal{T}_{99}$ than a brute-force search. Nevertheless, the quantum annealing algorithm with an antiferromagnetic trigger Hamiltonian for short annealing times and the new generation of the D-Wave systems result in a better scaling than that obtained by solving these problems using simulated annealing.

The paper is organized as follows. Section II gives a brief review of the theoretical aspects of quantum annealing and related concepts. In Sec. III we describe the 2-SAT problems that have been used for this study and briefly explain the methods used to obtain and analyze the results. Section IV discusses the results obtained from simulations, while in Sec. V we show the results obtained with the D-Wave systems. Finally, we summarize our observations in Sec. VI.

II. THEORETICAL BACKGROUND

This section aims at equipping the readers with the theoretical background necessary to understand the important aspects of, or related to, quantum annealing such as the recipe for the algorithm, the adiabatic theorem, the Landau-Zener formula, and the modifications to the standard algorithm for quantum annealing.

A. Quantum annealing and the adiabatic theorem

To employ quantum annealing to solve an optimization problem, we start the algorithm in the easy-to-prepare ground state of an initial Hamiltonian H_I. The system is then slowly swept towards the problem Hamiltonian H_P, which encodes the solution of the optimization problem in its ground state by means of the annealing parameter s, defined as $s = t/T_A$, where T_A is the annealing time. The time-dependent Hamiltonian has the form

$$H(s) = A(s)H_I + B(s)H_P, \tag{1}$$

where the functions $A(s)$ and $B(s)$ control the annealing scheme such that $A(0)/B(0) \gg 1$ and $A(1)/B(1) \ll 1$. For simplicity in our simulations, we choose the annealing scheme to be linear, i.e., $A(s) = 1 - s$ and $B(s) = s$. Frequently, the initial Hamiltonian is chosen to be

$$H_I = -\sum_{i=1}^{N} h_i^x \sigma_i^x, \tag{2}$$

while the problem Hamiltonian is of the Ising type,

$$H_P = -\sum_{i=1}^{N} h_i^z \sigma_i^z - \sum_{\langle i,j\rangle} J_{i,j}^z \sigma_i^z \sigma_j^z, \tag{3}$$

where σ_i^x and σ_i^z are the Pauli matrices, h_i^x and h_i^z are the applied fields acting along the x and z directions, respectively, $J_{i,j}^z$ is the coupling between the ith and jth spins, and $\langle i, j\rangle$ denotes the set of coupled spins; h_i^x is generally chosen to be 1.

The dynamics of the system described by this Hamiltonian is governed by the time-dependent Schrödinger equation (TDSE). Hence, the task of finding the solution of the optimization problem is equivalent to solving the TDSE

$$i\frac{\partial |\psi\rangle}{\partial t} = H(t)\,|\psi\rangle\,, \tag{4}$$

where we have set $\hbar = 1$. We use dimensionless quantities in our simulations.

The adiabatic theorem states that if the sweeping from the initial to the problem Hamiltonian is done slowly enough during the annealing, the system stays in the same instantaneous energy eigenstate as that in which the algorithm starts [47,53–55]. Therefore, if one starts in the ground state of the initial Hamiltonian, one reaches the state encoding the solution of the optimization problem at the end of the algorithm. This

requires [47]

$$T_A \gg \max_{0\leqslant s\leqslant 1} \frac{\left\| \langle 1(s)| \frac{dH}{ds} |0(s)\rangle \right\|}{\Delta(s)^2}, \tag{5}$$

where $|0(s)\rangle$ and $|1(s)\rangle$ are the ground state and first excited state of the instantaneous Hamiltonian, respectively, and $\Delta(s)$ is the energy gap between them.

As can be seen from Eq. (5), the annealing time required to reach the ground state of the problem Hamiltonian adiabatically depends crucially on the minimum energy gap $\Delta_{\min}$ between the ground state and the first excited state of the Hamiltonian, i.e., $\Delta = \min_{0\leqslant s\leqslant 1} \Delta(s)$. A Hamiltonian with a small minimum energy gap requires a long annealing time to keep the state of the system in the instantaneous ground state.

B. Landau-Zener theory

A test for gauging the performance of quantum annealing is to determine the probability of the final state being the required solution of the encoded problem with a given minimum energy gap and for a chosen annealing time. This probability will henceforth be referred to as the success probability.

The Landau-Zener theory describes the response of a two-level system under the action of a varying external magnetic field [56–58]. Considering a spin-1/2 particle in a time-dependent magnetic field $h(t) = ct$, where c is the rate of sweep and t varies from $-\infty$ to ∞, the Hamiltonian for the system is given by

$$H = -\Gamma\sigma_i^x - h(t)\sigma_i^z, \tag{6}$$

where Γ sets the scale of the energy splitting between the two levels [58]. When t is large and negative and $|h(t)| \gg \Gamma$, the spin-down state is the ground state of the Hamiltonian, while for large and positive t, the spin-up state is the ground state of the Hamiltonian. According to the Landau-Zener theory, the success probability after the sweep is

$$p = 1 - \exp\left(\frac{-\pi\Delta_{\min}^2}{4c}\right), \tag{7}$$

where $\Delta_{\min} = 2\Gamma$ is the minimum energy gap between the two levels and $c = dh/dt$. Although in this work we deal with systems which are more complex than a simple two-level system, if the chosen annealing time is sufficiently long, the system can be well approximated by a two-level system. Hence, the Landau-Zener formula can still be employed to determine the probability of an adiabatic evolution for such systems.

C. Addition of the trigger Hamiltonian

In order to investigate how introducing modifications to the standard algorithm for quantum annealing can affect its performance, we add a third term [9,52], the trigger Hamiltonian H_T, to the standard algorithm for quantum annealing. This term should vanish at the beginning and end of the annealing process so that the ground states of the initial Hamiltonian and problem Hamiltonian remain unaffected. Upon choosing a linear annealing scheme, we obtain

$$H(s) = (1-s)H_I + s(1-s)H_T + sH_P. \tag{8}$$

We have chosen the trigger Hamiltonian to have the same connectivity graph as that of the problem Hamiltonian, i.e.,

$$H_T = -\sum_{\langle i,j\rangle} J_{i,j}^x \sigma_i^x \sigma_j^x. \tag{9}$$

Furthermore, the trigger Hamiltonian can be of two types, the ferromagnetic trigger Hamiltonian, with $J_{i,j}^x = 1$, and the antiferromagnetic trigger Hamiltonian with $J_{i,j}^x = -1$.

III. PROBLEMS AND METHODS

In this section we describe the set of problems that we want to solve using quantum annealing. Next we explain the methods used to obtain both numerical and D-Wave results as well as the criteria that will be employed for the interpretation of these results.

A. 2-SAT problems

In this work we want to use quantum annealing to solve problems that are hard to solve with classical algorithms like simulated annealing. To accomplish this task, we construct sets of 2-SAT problems with varying problem size, with each problem having a unique satisfying assignment (selected using the brute-force search method). Moreover, the degeneracy of the first excited state grows exponentially as the size of the problems increases [43]. Such properties make these problems difficult to solve using simulated annealing.

A 2-SAT problem consists of a cost function F, involving N binary variables $x_i = 0, 1$ and a conjunction of M clauses such that

$$F = (L_{1,1} \vee L_{1,2}) \wedge (L_{2,1} \vee L_{2,2}) \wedge \cdots \wedge (L_{M,1} \vee L_{M,2}), \tag{10}$$

where $L_{\alpha,j}$, with $\alpha = 1, \ldots, M$ and $j = 1, 2$, is a variable x_i or its negation $\overline{x_i}$. A problem is considered to be satisfiable if one can find an assignment to the x_i's which makes the cost function true. The problem of finding a satisfying assignment to the cost function is equivalent to finding the ground state of the Hamiltonian

$$H_{2\text{-SAT}} = \sum_{\alpha=1}^{M} h_{2\text{-SAT}}(\epsilon_{\alpha,1}s_{i(\alpha,1)}, \epsilon_{\alpha,2}s_{i(\alpha,2)}), \tag{11}$$

constructed from a combination of the clauses of the 2-SAT problems, where $h_{2\text{-SAT}}(s_l, s_m) = (s_l - 1)(s_m - 1)$ and $i(\alpha, j)$ maps the jth literal from the αth clause to the index i of variable x_i for $\alpha = 1, \ldots, M$, $j = 1, 2$, and $i = 1, \ldots, N$. The variable $\epsilon_{\alpha,j} = 1$ if $L_{\alpha,j} = x_i$, while $\epsilon_{\alpha,j} = -1$ if $L_{\alpha,j} = \overline{x_i}$ [43,46]. These spins are further replaced by the quantum spin operator σ_i^z for using quantum annealing to find the minimum-energy state of the Hamiltonian.

We present results for 13 sets of 2-SAT problems, each corresponding to an N, with N ranging from 6 to 18, and $M = N + 1$. The sets corresponding to small N ($N < 10$) have 100 problems each, while larger sets have 1000 problems for each N. However, it was observed that some problems had the same graph as another problem belonging to the set, and therefore such redundancies have been removed from every set. As a result, the sets corresponding to $N < 10$ have more

than 70 problems each, while the sets with $N \geqslant 10$ have more than 900 problems, except for sets with $N = 15$ and 18, which have 557 and 789 problems, respectively.

B. Analysis of numerical results

Focusing now on the numerical analysis of our study, this section describes three observables that are used as a basis for determining the complexity of quantum annealing for solving our problems in Sec. IV. We perform this analysis for three quantum annealing algorithms, i.e., using the Hamiltonian given by Eq. (1), the one given by Eq. (8) with the ferromagnetic trigger Hamiltonian, and that given by the Hamiltonian (8) with the antiferromagnetic trigger Hamiltonian. We use the three quantum annealing algorithms to solve 13 sets of 2-SAT problems, each corresponding to a different N.

1. Minimum energy gaps

In the adiabatic theorem [Eq. (5)] and the Landau-Zener formula [Eq. (7)], the minimum energy gap is a decisive quantity for determining the performance of quantum annealing in the adiabatic regime. We employ the Lanczos algorithm [59] to obtain the energy spectra of the problem Hamiltonians. We investigate two aspects of the minimum energy gap: its distribution for a fixed problem size and its scaling as a function of the problem size. We use the distribution functions given in Appendix A to fit the obtained minimum energy gap distributions.

In order to inspect the scaling, we calculate the deciles for the minimum energy gaps for each quantum annealing Hamiltonian, given by Eq. (1) or (8) (using the ferromagnetic or the antiferromagnetic trigger Hamiltonian), with N ranging from 6 to 18. The problems which have a minimum energy gap smaller than the first decile $D1$ represent the hardest problems of the set, while the problems with a larger minimum energy gap than the ninth decile $D9$ represent the easiest problems of the set. We obtain the scaling of the minimum energy gaps by fitting suitable functions to the deciles in the asymptotic limit.

According to the adiabatic theorem [Eq. (5)], this analysis can be extrapolated to provide an estimate for the annealing time required to ensure an adiabatic evolution of the state of the system for a given minimum energy gap. According to the theorem, this annealing time is inversely proportional to $\Delta_{\min}^2$,

$$T_A \propto \frac{1}{\Delta_{\min}^2}. \tag{12}$$

If the correlation length $\xi = 1/\Delta_{\min}$ increases exponentially as a function of the problem size, then the runtime required to keep the evolution adiabatic is also expected to grow exponentially with an exponent twice as large. Therefore, this gives an estimate for how the computation time should scale if the evolution of the state is adiabatic.

2. Success probability

The next important observable for our analysis is the success probability, which is obtained by calculating the square of the overlap of the resulting state at the end of the annealing process with the known ground state of the problem Hamiltonian. We use the second-order Suzuki-Trotter product formula algorithm [60–63] to simulate the dynamics of quantum annealing. These simulations are performed for three annealing times, $T_A = 10$, 100, and 1000, which are dimensionless since $\hbar$ has been set equal to 1.

As indicated by our previous study [52], for our problems, the annealing time $T_A = 10$ can be too short for the state of the system to follow the ground state adiabatically, especially for the problem sets with larger N. This gives way to certain nonadiabatic mechanisms to be involved in the evolution of the state of the system. On the other hand, $T_A = 1000$ was found to be sufficiently long for the success probability to follow the Landau-Zener formula for a majority of the problems. The annealing time $T_A = 100$ is the intermediate annealing time for which the difficult problems might still exhibit a nonadiabatic evolution, while the systems with larger minimum energy gaps evolve adiabatically.

We obtain the success probabilities for the three quantum annealing algorithms and for the three chosen annealing times and plot the resulting distributions. For all the results shown, the raw success probabilities p obtained from the simulations are transformed such that $\langle P_{\text{succ}} \rangle = 1/2$, where

$$P_{\text{succ}} = 1 - (1 - p)^R. \tag{13}$$

The parameter R can be interpreted as the number of repetitions, or a scaling factor for the annealing time, required to shift the average success probability of the set to 0.5. For long annealing times, it is possible to derive distributions for the success probability for a set of problems, given the corresponding minimum energy gap distributions. Such a mapping is derived in Appendix B.

3. Time to solution

Finally, we discuss the third metric for determining the complexity of quantum annealing, the time to solution. It is the runtime required to obtain the ground state at least once in multiple runs of the algorithm with a certain probability P_{target} and is given by

$$\mathcal{T} = \frac{\ln(1 - P_{\text{target}})}{\ln(1 - p)} T_A, \tag{14}$$

where the success probability p is obtained with a single run of the algorithm with annealing time T_A. We define $\mathcal{T}_{99}$ as the runtime required to obtain at least one solution with 99% certainty, i.e., $\mathcal{T}_{99} = \mathcal{T}(P_{\text{target}} = 0.99)$.

Like in the case of the minimum energy gaps, we plot the deciles for $\mathcal{T}_{99}$ as a function of the problem size ($10 \leqslant N \leqslant 18$). In this case, the easier problems of the set have a runtime smaller than the first decile, while the problems having a runtime larger than the ninth decile correspond to the hard cases. To determine the scaling of $\mathcal{T}_{99}$ an appropriate function is fit to the deciles in the asymptotic limit.

If the annealing time is long enough for an adiabatic evolution, the success probability is mainly determined by the minimum energy gap between the ground state and the first excited state of the Hamiltonian. However, for a nonadiabatic evolution the exact energy spectrum of the problem also becomes relevant. For example, the occurrence of an even number of comparably small anticrossings between the

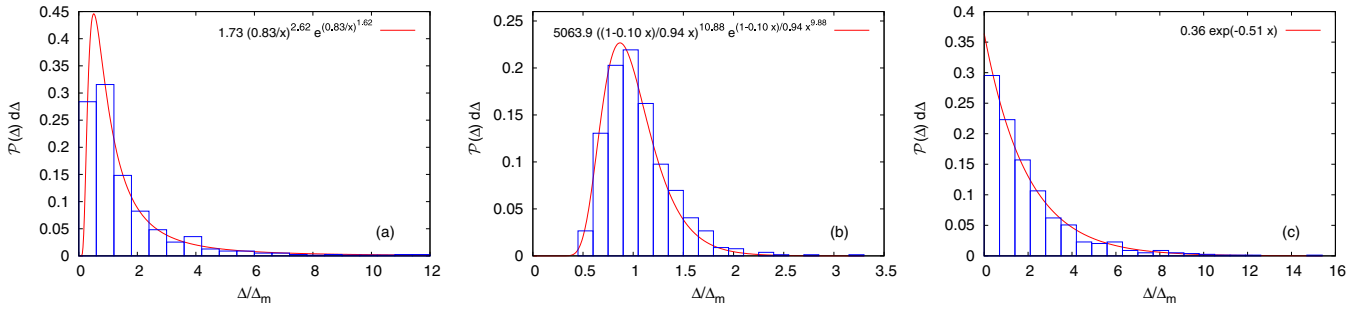

FIG. 1. Median-normalized minimum energy gap distributions $\mathcal{P}(x)dx$ for (a) the standard quantum annealing Hamiltonian (1), (b) the Hamiltonian (8) with the ferromagnetic trigger Hamiltonian, and (c) the Hamiltonian (8) with the antiferromagnetic trigger Hamiltonian, for the problem set with $N = 18$, where $x = \Delta/\Delta_m$, with Δ_m the median minimum energy gap of the set.

two lowest energy levels can be beneficial for the final success probability [52]. Such observations cannot be accounted for within the theoretical models like Landau-Zener theory and the adiabatic theorem. It therefore becomes interesting to compare the scaling of the theoretical runtime with the numerically obtained $\mathcal{T}_{99}$ scaling in order to understand the ways in which the nonadiabatic mechanisms can contribute to the scaling.

C. Analysis of the D-Wave results

This section briefly describes how the D-Wave quantum annealer is employed to solve the sets of problems and how the obtained results (shown in Sec. V) are analyzed. Currently, D-Wave offers systems with two types of quantum chip topologies. The first is the Chimera topology available on the DW_2000Q_6 system (DW2000Q), while the more recent and better connected one is the Pegasus topology available on the Advantage_system1.1 system (DWAdv) [26]. To find the ground state of our Ising Hamiltonian using the D-Wave annealer, the problem Hamiltonian needs to be mapped to the working graph of the system. However, it is possible that a Hamiltonian cannot be directly embedded in the system and requires two or more physical qubits to be grouped together to represent a logical qubit of the Hamiltonian instead. Since the Pegasus topology has a higher connectivity compared to that of the Chimera topology, most of the problems could be directly embedded in DWAdv, whereas only approximately half of the cases have a direct mapping on DW2000Q. For example, for the set corresponding to $N = 17$, only 489 out of 913 problems have a direct mapping on DW2000Q, but this number increases to 854 on DWAdv.

We employ both DW2000Q and DWAdv systems to solve nine sets of problems ($10 \leqslant N \leqslant 18$) and choose annealing times of 4, 20, and 100 μs. The success probabilities in this case are determined by finding the ratio of the outcomes with the correct ground-state energy to the total number of samples. For annealing times of 4 and 20 μs, the total number of samples is chosen to be 10 000, while there are 2000 samples for $T_A = 100$ μs. We gauge the performance of the D-Wave systems by observing the success probability distributions by mapping the raw success probability p to success probability P_{succ} using Eq. (13) and the scaling of $\mathcal{T}_{99}$ and compare it to the results obtained from the simulations.

It should be mentioned at this point that the annealing times available on the D-Wave systems are significantly longer than those feasible for the simulations. Moreover, noise and temperature effects play a significant role in their performance, and the annealer is therefore not expected to behave adiabatically, even for sufficiently long annealing times [64,65].

IV. NUMERICAL RESULTS

In this section we present the simulation results for the three previously described observables, which can help us understand the complexity of the quantum annealing algorithm in solving the selected problems. The following sections discuss these observables one by one.

A. Minimum energy gap analysis

We begin by addressing the results obtained for the static quantifier of quantum annealing, i.e., the minimum energy gap where we have further separated the distributions of the minimum energy gaps from the scaling results as a function of the problem size.

1. Minimum energy gap distributions

Figure 1(a) shows the median-normalized minimum energy gap distributions for the standard quantum annealing Hamiltonian given by Eq. (1), for the problem set with $N = 18$. The corresponding distributions for problem sets with $N = 16, 17$ are shown in Figs. 2(a) and 2(b). It can be seen that the distribution agrees well with the Fréchet function (see Appendix A) and that the value of the variable k [see Eq. (A1)] decreases as the problem size becomes larger, tending towards the value of 1 as N increases.

The minimum energy gap distribution for the quantum annealing Hamiltonian given by Eq. (8) with the ferromagnetic trigger Hamiltonian, as shown in Fig. 1(b), differ significantly from the distributions for the standard quantum annealing Hamiltonian given by Eq. (1). This is also the case for the problem sets corresponding to $N = 16, 17$ shown in Figs. 2(c) and 2(d), respectively. Previous studies have suggested that the addition of the ferromagnetic trigger Hamiltonian to the standard Hamiltonian for quantum annealing can result in an enlargement of the minimum energy gaps for almost all the problems belonging to the studied sets [52]. The distribution therefore is very different from that of the standard

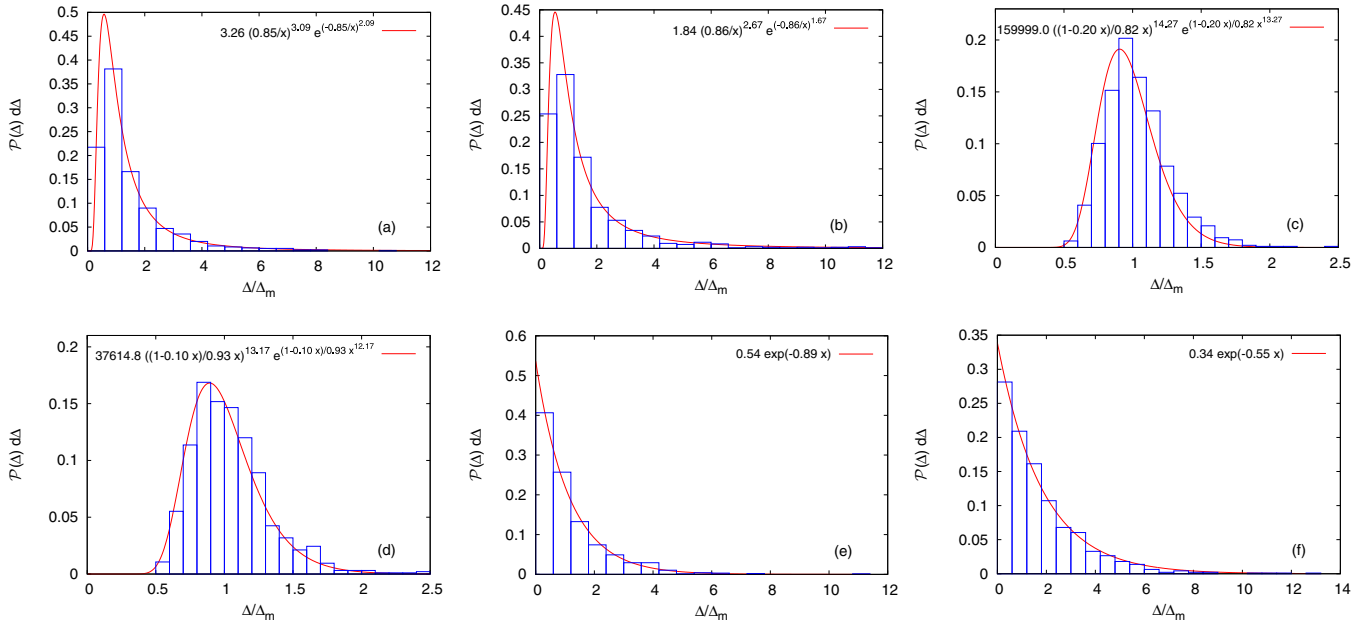

FIG. 2. Median-normalized minimum energy gap distributions $\mathcal{P}(x)dx$ for the quantum annealing Hamiltonian given by (a) and (b) Eq. (1), (c) and (d) Eq. (8) with the ferromagnetic trigger Hamiltonian, and (e) and (f) Eq. (8) with the antiferromagnetic trigger Hamiltonian, for problem sets with (a), (c), and (e) $N = 16$ and (b), (d), and (f) $N = 17$, where $x = \Delta/\Delta_m$, with Δ_m the median minimum energy gap of the set.

quantum annealing Hamiltonian and is similar to the normal distribution.

To obtain the fits for the minimum energy gap distribution, we fit translated Weibull functions [Eq. (A3)] to the distribution of correlation length $\xi = 1/\Delta_{\min}$. In this case, the parameter μ in Eq. (A3) can be interpreted as the shift due to adding the ferromagnetic trigger Hamiltonian. By setting the parameters μ, b, and k obtained from fitting the translated Weibull function to the median-normalized correlation length distribution, we fit the transformed, translated Weibull function [Eq. (A4)] to the corresponding median-normalized minimum energy gap distribution by the parameter a. The resulting fits match the form of the distribution well.

Finally, the median-normalized minimum energy gap distribution for the quantum annealing Hamiltonian given by Eq. (8) with the antiferromagnetic trigger Hamiltonian for $N = 18$ is shown in Fig. 1(c), while that for problem sets with $N = 16$ and 17 is shown in Figs. 2(e) and 2(f), respectively. For this case, exponentially decaying functions match the distribution well. This function is equivalent to the Weibull distribution with $k = 1$.

At this point, it should be noted that three distinct minimum energy gap distributions are obtained for the three quantum annealing Hamiltonians discussed. Therefore, according to Eq. (B4), we can expect to obtain three kinds of success probability distributions for the three quantum annealing Hamiltonians.

2. *Scaling of minimum energy gaps*

In order to investigate the complexity of the quantum annealing algorithm in solving the set of problems considered in this work, we now turn to the scaling aspect of the minimum energy gaps as a function of the problem size. Figure 3 shows the scaling of the median minimum energy gaps for the three types of quantum annealing Hamiltonians examined in this study. The odd deciles for the minimum energy gaps as a function of the problem size for the three annealing Hamiltonians are given in Fig. 4. It can be observed that for all three cases, the decile values decrease exponentially as a function of the problem size in the asymptotic limit. Hence, we use exponents obtained by fitting the exponential functions $\Delta_{\min} = De^{-r_\Delta N}$ to the deciles and also the median, to determine the scaling of the minimum energy gaps. For all three

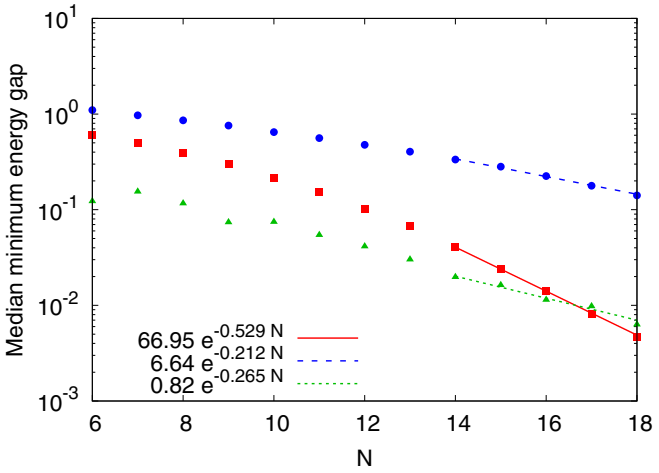

FIG. 3. Scaling of median minimum energy gaps for the quantum annealing Hamiltonian given by Eq. (1) (squares), the quantum annealing Hamiltonian given by Eq. (8) with the ferromagnetic trigger Hamiltonian (circles), and the quantum annealing Hamiltonian given by Eq. (8) with the antiferromagnetic trigger Hamiltonian (triangles).

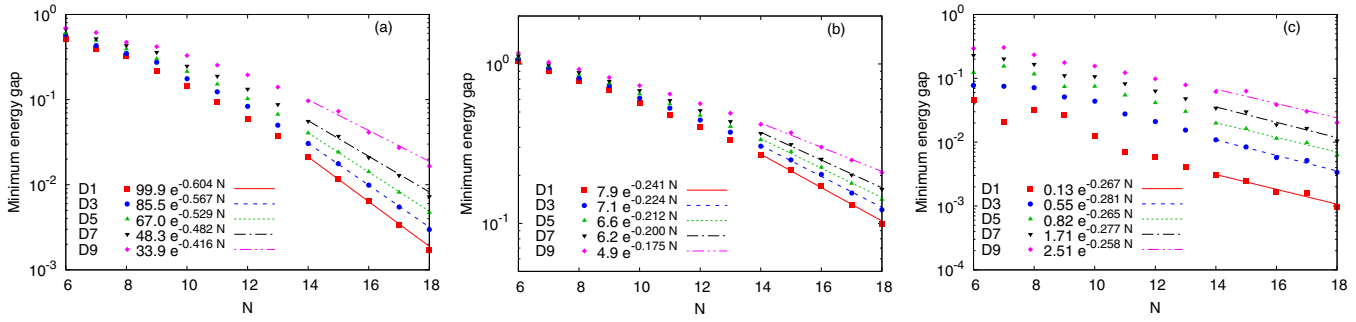

FIG. 4. Deciles for the minimum energy gaps for the quantum annealing Hamiltonian given by (a) Eq. (1), (b) Eq. (8) with the ferromagnetic trigger Hamiltonian, and (c) Eq. (8) with the antiferromagnetic trigger Hamiltonian.

quantum annealing Hamiltonians, the fitting is done for the sets with $N \geqslant 14$.

The exponential vanishing of the minimum energy gaps with the increasing size of the problems in the asymptotic limit confirms the hardness of these problems. From Fig. 4 it can also be seen that while for the quantum annealing Hamiltonians given by Eqs. (1) and (8) with the ferromagnetic trigger Hamiltonian the exponent r_Δ grows monotonically as one goes from $D1$ to $D9$, for the Hamiltonian given by Eq. (8) with the antiferromagnetic trigger Hamiltonian the exponents stay similar for all the deciles. The median minimum energy gap, given by $D5$, scales with a rate of $r_\Delta = -0.529$ for the standard quantum annealing Hamiltonian given by Eq. (1), whereas $r_\Delta = -0.212$ and -0.265 for the quantum annealing Hamiltonian given by Eq. (8) with the ferromagnetic trigger Hamiltonian and the antiferromagnetic trigger Hamiltonian, respectively. Therefore, the addition of both triggers improves the scaling of the median minimum energy gap despite the finding that adding the antiferromagnetic trigger can either enlarge or reduce the minimum energy gaps between the ground state and first excited states of a Hamiltonian [9,52].

Using Eq. (12), we extend this analysis to obtain the scaling of the theoretical runtime, which provides an estimate for how the computation time required for ensuring an adiabatic evolution of the state of the system grows as the size of the problem increases. We therefore expect that the median runtime should scale with a rate of $r_{\mathrm{TR}} = 1.058$ for the quantum annealing algorithm using the Hamiltonian (1) if one were to fit functions of the form $T_A = D\exp(r_{\mathrm{TR}}N)$ to the corresponding plots. Similarly, for the quantum annealing algorithm using the Hamiltonian (8) with the ferromagnetic trigger Hamiltonian, the median runtime is expected to grow with an exponent $r_{\mathrm{TR}} = 0.424$, while for the algorithm using the Hamiltonian (8) with the antiferromagnetic trigger Hamiltonian, r_{TR} is expected to be 0.530 in the median.

Since a brute-force search for the ground state of the problem Hamiltonian scales as 2^N with the Hilbert space, and therefore with an exponent of $\ln(2) = 0.693$, even a simple random generation of the eigenstates can yield the ground state of the problem Hamiltonian faster than the standard algorithm for quantum annealing, i.e., with the Hamiltonian (1). However, the expected runtime improves upon adding both trigger Hamiltonians, not only in comparison to the standard quantum annealing algorithm, but also compared to the brute-force search, especially for the quantum annealing algorithm with the ferromagnetic trigger Hamiltonian.

B. Success probability distributions

Having discussed the static quantifier of the quantum annealing search complexity for our problems, we now move on to address a dynamic quantifier: the success probability obtained using the three quantum annealing Hamiltonians considered in this work for three annealing times.

Figures 5(a)–5(c) show the mapped success probability distributions obtained, according to Eq. (13), from the quantum annealing algorithm with the Hamiltonian (1), for problem sets with $N = 18$ and annealing times of $T_A = 10, 100, 1000$, respectively. For the success probability distributions corresponding to the problem set with $N = 17$ for the three annealing Hamiltonians used in this work, see Fig. 6. Using the energy scale of a D-Wave annealer, this translates to annealing times of 0.5, 5, and 50 ns, respectively. It can be observed that the resulting distribution is bimodal for all the annealing times and both problem sets. Although not for 2-SAT problems, similar results have been obtained for the success probability distribution for solving spin-glass problems using simulated quantum annealing and a 108-qubit D-Wave One system [31].

A similar treatment of the success probability distributions obtained for the quantum annealing algorithm using the Hamiltonian (8) with the ferromagnetic trigger Hamiltonian, however, results in unimodal distributions, as shown in Figs. 5(d)–5(f). This is in contrast with the observations in [31], where a unimodal distribution was obtained only for the success probability of solving spin-glass problems using simulated annealing.

Interestingly, the mapped success probability distributions for the quantum annealing algorithm using the Hamiltonian (8) with the antiferromagnetic trigger Hamiltonian result in two kinds of distributions, depending on the chosen annealing time. It can be seen from Figs. 5(g)–5(i) that the distributions corresponding to $T_A = 10$ seem rather constant, whereas on increasing the annealing time, like in [31], the distributions show bimodality. It should be noted that this instance does not correspond to the case for which the Landau-Zener theory predicts a constant distribution (Appendix B). The difference originates from the fact that the theoretical mapping between the distributions for the

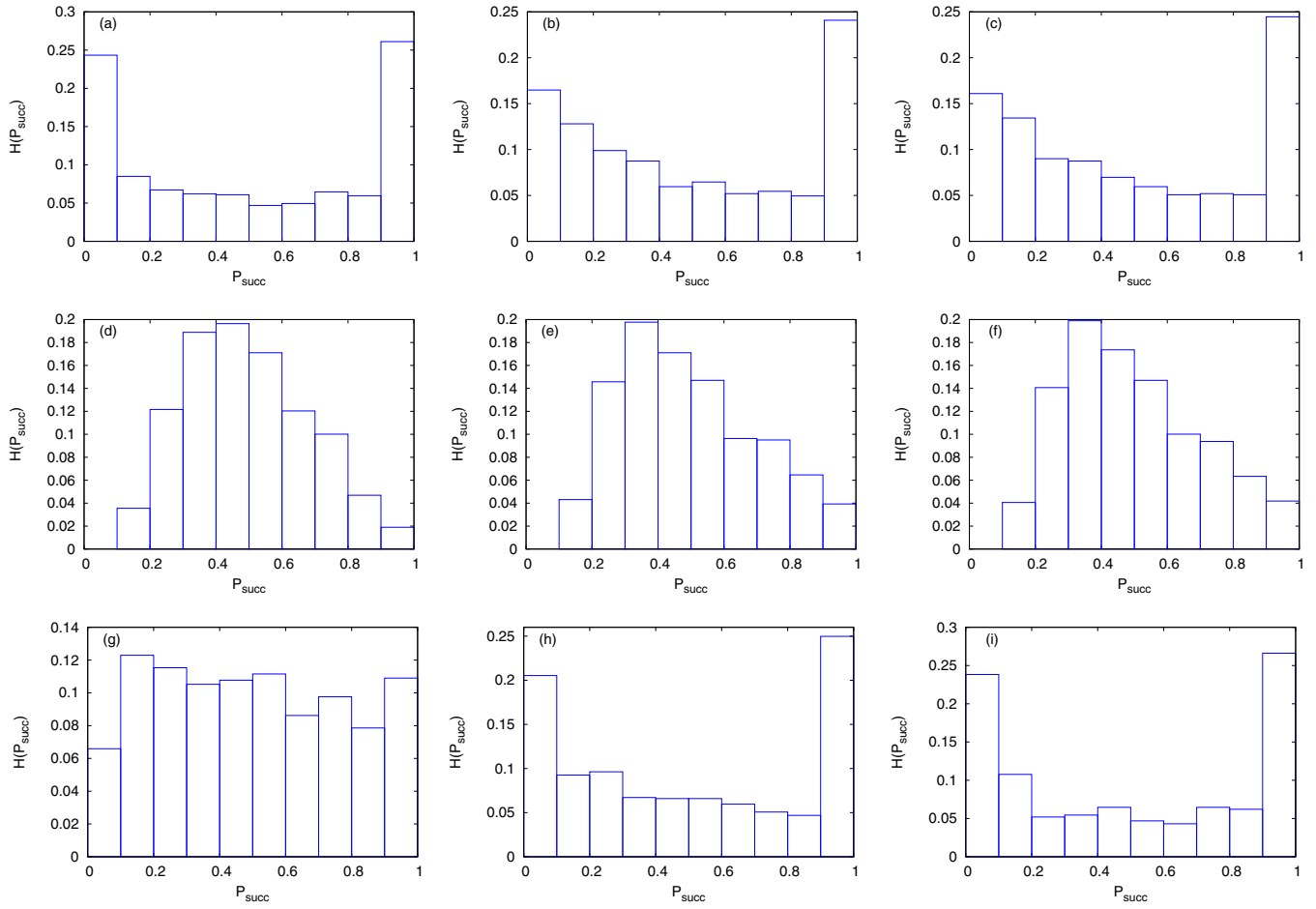

FIG. 5. Success probability distributions obtained for the quantum annealing algorithm using (a)–(c) the Hamiltonian (1), (d)–(f) the Hamiltonian (8) with the ferromagnetic trigger Hamiltonian, and (g)–(i) the Hamiltonian (8) with the antiferromagnetic trigger Hamiltonian, for the problem set with $N = 18$ for (a), (d), and (g) $T_A = 10$; (b), (e), and (h) $T_A = 100$; and (c), (f), and (i) $T_A = 1000$.

minimum energy gap and the success probability utilizes the Landau-Zener formula, which only holds in the adiabatic limit, i.e., for long annealing times. This, however, is not the case here as for $T_A = 10$, especially upon adding the antiferromagnetic trigger Hamiltonian, nonadiabatic mechanisms can additionally be responsible for improving the success probability, as can be confirmed from [52]. Nevertheless, the success probability distributions from the simulations for the dynamics of quantum annealing can result in three types of distributions, i.e., unimodal, bimodal and constant distributions.

C. Scaling of $\mathcal{T}_{99}$

In this section we present the scaling results for another dynamic quantifier of the quantum annealing search complexity, the time to solution with 99% certainty, obtained by using Eq. (14). Figure 7 shows the scaling of the median $\mathcal{T}_{99}$ obtained from the success probabilities for the three quantum annealing Hamiltonians considered in this work, with $10 \leqslant N \leqslant 18$ and for $T_A = 10, 100, 1000$. The corresponding odd deciles for the $\mathcal{T}_{99}$ as a function of the problem size are given in Fig. 8.

As a first observation, it should be noted that, as expected, the runtime for all the deciles increases exponentially as the problem size increases in the asymptotic limit, and thus the fitting function $\mathcal{T}_{99} = D \exp(r_{\mathcal{T}_{99}} N)$ has been used here [see Figs. 8(a)–8(c)]. It can also be seen that some data points corresponding to the median $\mathcal{T}_{99}$ for $T_A = 100$ and 1000 are almost identical in Figs. 7(a) and 7(b). Since for these annealing times the Landau-Zener formula holds, the $\mathcal{T}_{99}$ coincides with the annealing time required to obtain the success probability of 0.99. Second, the median $\mathcal{T}_{99}$ scales with a rate $r_{\mathcal{T}_{99}} = 0.530$ for $T_A = 10$, but increases to $r_{\mathcal{T}_{99}} = 1.170$ and 1.205 as the annealing time is increased to 100 and 1000, respectively. This is an interesting observation as it suggests that for long annealing times, the runtime required to obtain at least one solution with 99% probability scales with a similar exponent as predicted by the adiabatic theorem for the runtime as a function of the minimum energy gaps ($r_{\mathrm{TR}} = 1.058$ for the standard quantum annealing algorithm, as given in Sec. IV A 2) and thus worse than the brute-force search. For the short annealing time, however, the exponent is significantly smaller than the theoretical prediction and is also better than the brute-force search. This trend is also observed for the other two quantum annealing algorithms using the Hamiltonian (8), with

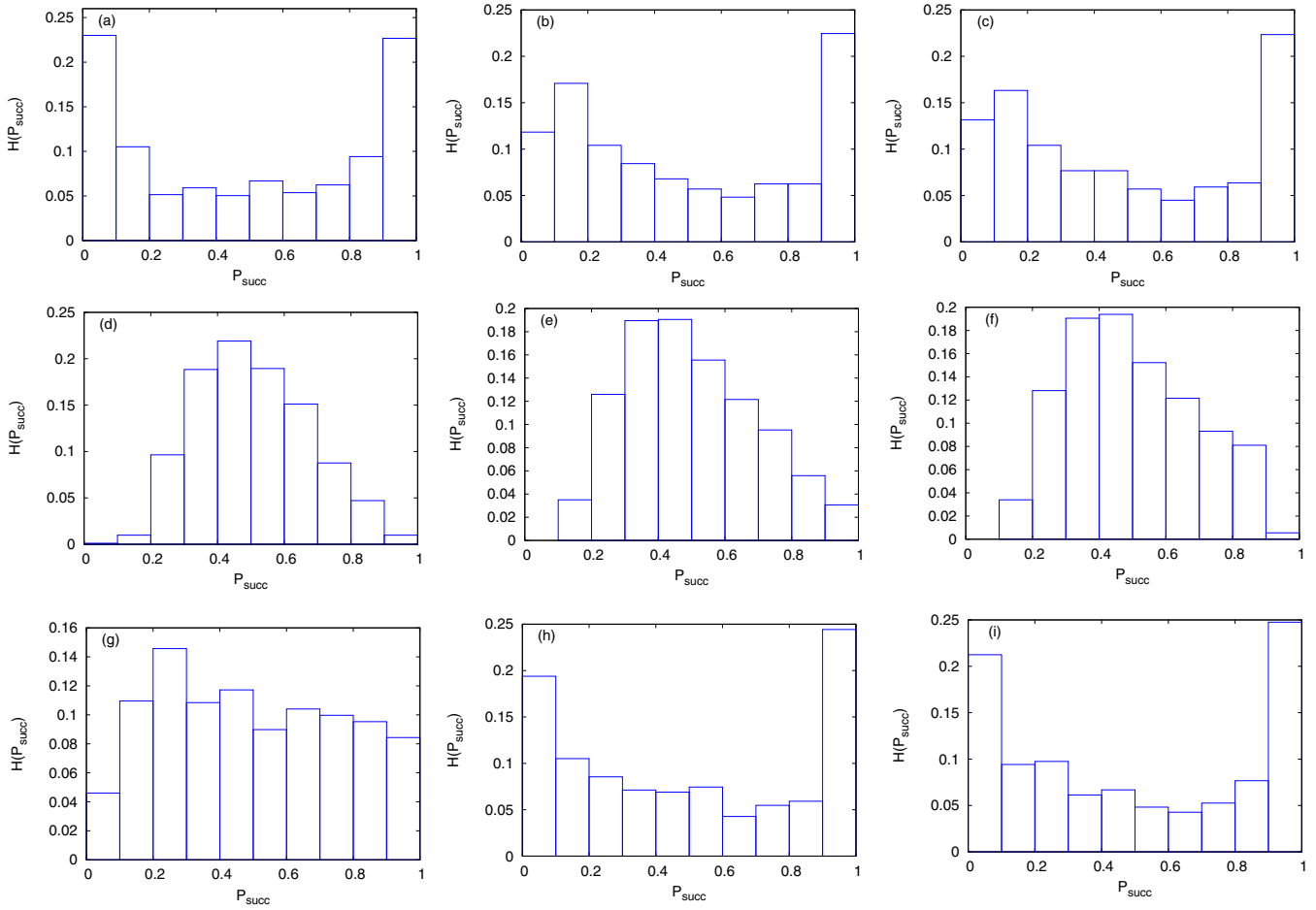

FIG. 6. Success probability distributions obtained for the quantum annealing given by (a)–(c) Eq. (1), (d)–(f) Eq. (8) with the ferromagnetic trigger Hamiltonian, and (g)–(i) Eq. (8) with the antiferromagnetic trigger Hamiltonian, for the problem set with $N = 17$ for (a) and (d) $T_A = 10$, (b) and (e) $T_A = 100$, and (c) and (f) $T_A = 1000$.

the ferromagnetic [Fig. 7(b)] and the antiferromagnetic trigger Hamiltonian [Fig. 7(c)], and can be explained as follows. The annealing time $T_A = 10$ is not long enough for the state of the system to evolve adiabatically, and hence the nonadiabatic mechanism of fast annealing can play a role in improving the success probabilities [52], making the exponent of the scaling of the median $\mathcal{T}_{99}$ smaller. Upon increasing the annealing time, the state of the system follows the adiabatic theorem, and therefore the dynamically obtained runtimes agree well with the theoretically predicted runtimes. It should nevertheless be noted that these observations have been found for the given set of hard 2-SAT problems, for which the ideal adiabatic evolution scales poorly compared even with the brute-force search.

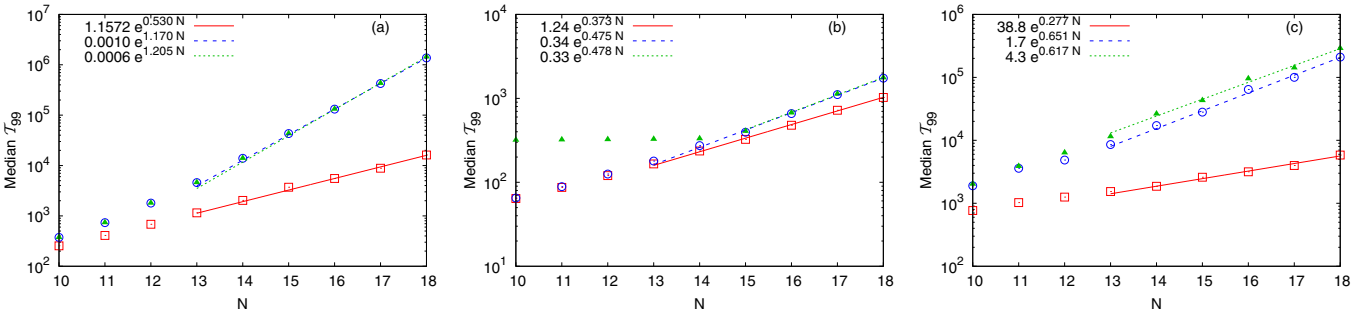

FIG. 7. Scaling of the median $\mathcal{T}_{99}$ for the quantum annealing Hamiltonian given by (a) Eq. (1), (b) Eq. (8) with the ferromagnetic trigger Hamiltonian, and (c) Eq. (8) with the antiferromagnetic trigger Hamiltonian, for $T_A = 10$ (squares), $T_A = 100$ (circles), and $T_A = 1000$ (triangles).

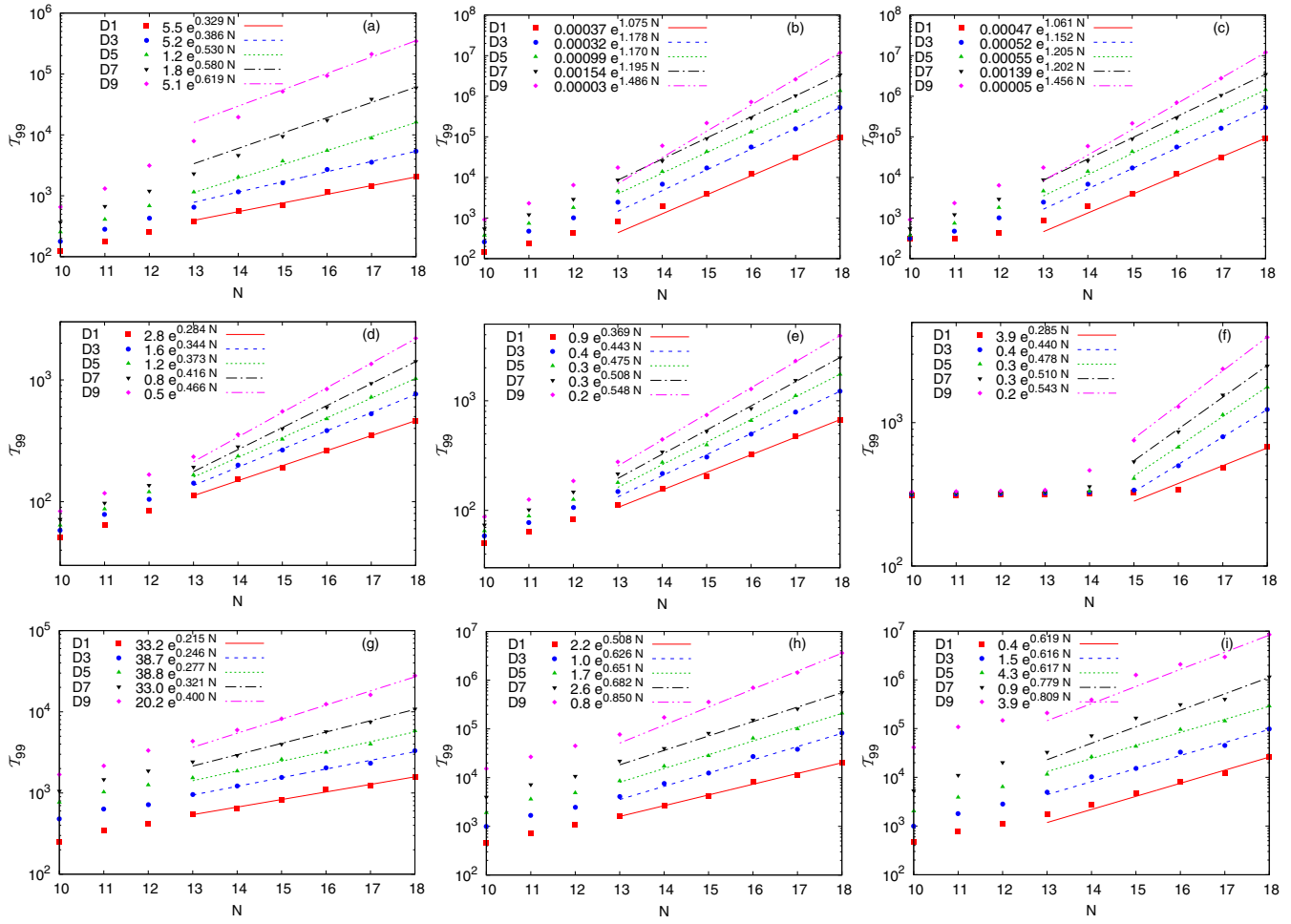

FIG. 8. Deciles for $\mathcal{T}_{99}$ for the quantum annealing Hamiltonian given by (a)–(c) Eq. (1), (d)–(f) Eq. (8) with the ferromagnetic trigger Hamiltonian, and (g)–(i) Eq. (8) with the antiferromagnetic trigger Hamiltonian for (a), (d), and (g) $T_A = 10$; (b), (e), and (h) $T_A = 100$; and (c), (f), and (i) $T_A = 1000$.

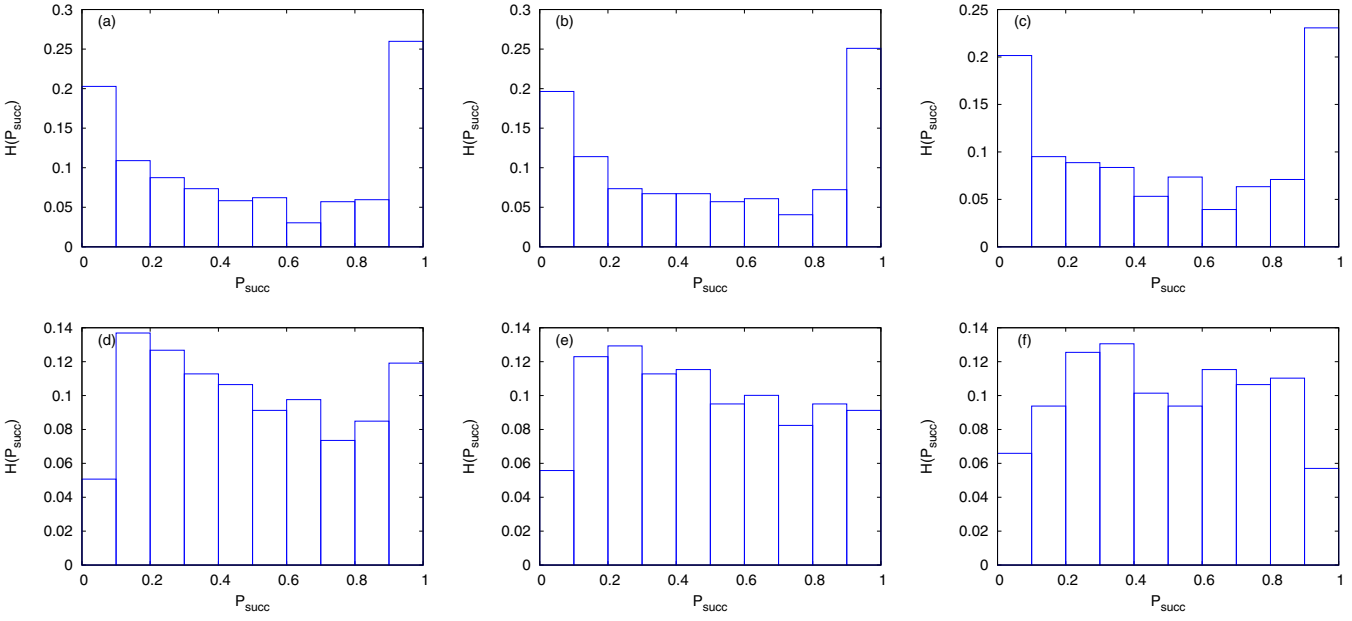

FIG. 9. Success probability distributions obtained using (a)–(c) DW2000Q and (d)–(f) DWAdv for the problem set with $N = 18$ for (a) and (d) $T_A = 4\ \mu$s, (b) and (e) $T_A = 20\ \mu$s, and (c) and (f) $T_A = 100\ \mu$s.

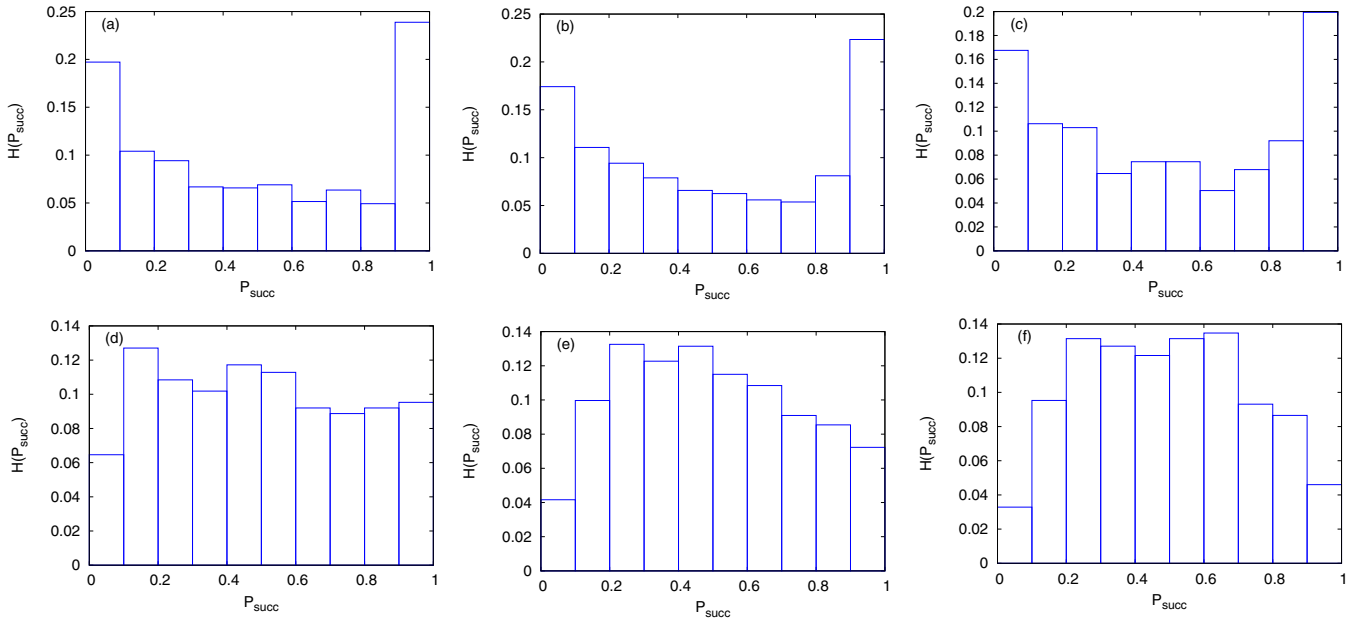

FIG. 10. Success probability distributions obtained using (a)–(c) DW2000Q and (d)–(f) DWAdv for the problem set with $N = 17$ for (a) and (d) $T_A = 4\ \mu$s, (b) and (e) $T_A = 20\ \mu$s, and (c) and (f) $T_A = 100\ \mu$s.

Additionally, by comparison of the algorithms with the three Hamiltonians, it can be seen that for the short annealing time of $T_A = 10$, the quantum annealing algorithm using the Hamiltonian (8) with the antiferromagnetic trigger Hamiltonian results in the best scaling ($r_{\mathcal{T}_{99}} = 0.277$ for the median $\mathcal{T}_{99}$). This is the regime where nonadiabatic mechanisms can play a significant role in the evolution of the system and the addition of the antiferromagnetic trigger enhances the nonadiabatic effects, thus improving the scaling. On the other hand, in the long annealing time limit, where the evolution is mainly adiabatic, quantum annealing using the Hamiltonian (8) with the ferromagnetic trigger Hamiltonian shows the best scaling ($r_{\mathcal{T}_{99}} = 0.475$ for $T_A = 100$ for median $\mathcal{T}_{99}$), consistent with the scaling obtained for the minimum energy gaps.

We can also observe that even for longer annealing times, the exponent $r_{\mathcal{T}_{99}}$ slightly varies from the theoretically predicted r_{TR}. To understand the reason for such a deviation, it can be noted from the success probability versus minimum energy plots in [52] that for our set of problems, the exponents of the minimum energy gap in the Landau-Zener formula are slightly different from 2 for the three quantum annealing Hamiltonians.

V. D-WAVE RESULTS

Finally, in this section we perform an analysis with the data obtained with the two D-Wave systems similar to that performed with the numerical results, by examining the success probability distributions and the scaling of $\mathcal{T}_{99}$.

A. Success probability distributions

Using Eq. (13), we map the raw success probabilities p such that $\langle P_{\mathrm{succ}} \rangle = 1/2$, as was done for the numerical results. Figures 9(a)–9(c) show the mapped success probability distributions for the problem set with $N = 18$ and annealing times $T_A = 4, 20, 100\ \mu$s using DW2000Q. Figure 10 shows the success probability distributions obtained from the two systems for the problem set with $N = 17$. It can be seen that for all annealing times, the distribution is always bimodal for DW2000Q, as was the numerically obtained success probability distribution using the standard quantum Hamiltonian given in Eq. (1).

Interestingly, the mapped success probability distributions for the same problem sets and annealing times but obtained with DWAdv are significantly different, as shown in Figs. 9(d)–9(f). These distributions are not bimodal, but instead are closer to unimodal and constant distributions. Such distributions were also obtained from the simulations of the dynamics of quantum annealing using the Hamiltonian (8) with the ferromagnetic and the antiferromagnetic trigger. However, the similar results from the simulations correspond to quantum annealing Hamiltonians different from the standard Hamiltonian implemented by D-Wave. Therefore, unlike the simulations, the D-Wave systems are not ideal and many other effects, such as temperature and noise, play a major role during the evolution of the system.

B. Scaling of $\mathcal{T}_{99}$

We discuss the scaling of the deciles for $\mathcal{T}_{99}$, as was done in Sec. IV C, from the success probabilities obtained with the two D-Wave systems. In calculating the deciles for $\mathcal{T}_{99}$, we have omitted the problems which could not be directly embedded in the D-Wave system in order to have a fair comparison with the scaling results obtained from the simulations.

We begin with Fig. 11(a), which shows the median $\mathcal{T}_{99}$ obtained from the success probabilities using DW2000Q. In this case too, in the asymptotic limit the $\mathcal{T}_{99}$ deciles (shown in Fig. 12) are found to increase exponentially as the problem size increases and hence are fit to functions $\mathcal{T}_{99} = D \exp(r_{\mathcal{T}_{99}} N)$. The exponents $r_{\mathcal{T}_{99}}$ obtained from the

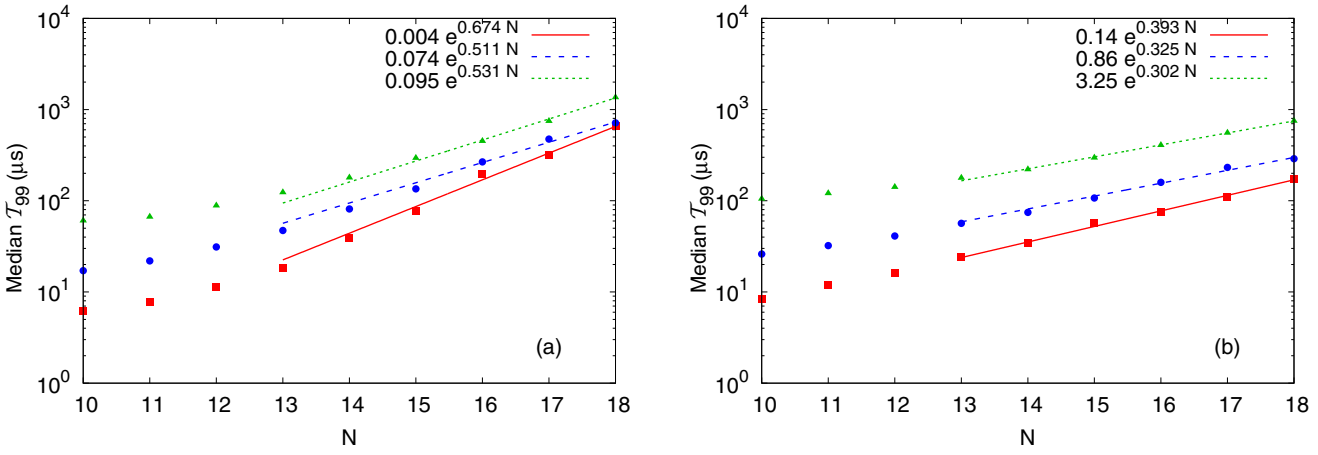

FIG. 11. Scaling of the median $\mathcal{T}_{99}$ for the cases with a native embedding on (a) DW2000Q and (b) DWAdv for $T_A = 4$ μs (squares), $T_A = 20$ μs (circles), and $T_A = 100$ μs (triangles).

fitting for the scaling of the median are 0.674, 0.511, and 0.531 for annealing times of 4, 20, and 100 μs, respectively. These values are better than the theoretical estimate for the runtime obtained from the adiabatic theorem ($r_{\mathrm{TR}} = 1.086$ from Sec. IV A 2) and better than the exponent for the brute-force search. Moreover, for annealing times 20 and 100 μs, the scaling exponents are similar to the scaling rate of the numerical $\mathcal{T}_{99}$ for the quantum annealing algorithm using the Hamiltonian (1) in the fast annealing limit ($r_{\mathcal{T}_{99}} = 0.530$ for $T_A = 10$ in Sec. IV C). This behavior can be explained on the basis of the noise present in the D-Wave system, which can give way to several nonadiabatic mechanisms improving the success probability.

A similar treatment of the median $\mathcal{T}_{99}$ obtained from the success probabilities using DWAdv results in an even better scaling, as shown in Fig. 11(b). In this case, $r_{\mathcal{T}_{99}}$ obtained from the fits to the median $\mathcal{T}_{99}$ is found to be 0.393, 0.325, and 0.302 for annealing times of 4, 20 and 100 μs. Although there is a need for further research, the topological differences between the connectivity of the qubits in the two D-Wave systems can offer a plausible explanation for the dissimilarity between the scaling results from the two systems. While a qubit in DW2000Q has a connectivity of 6, in DWAdv each qubit is connected to 15 other qubits. This can lead to additional noise being present in DWAdv, which can contribute towards a better scaling performance.

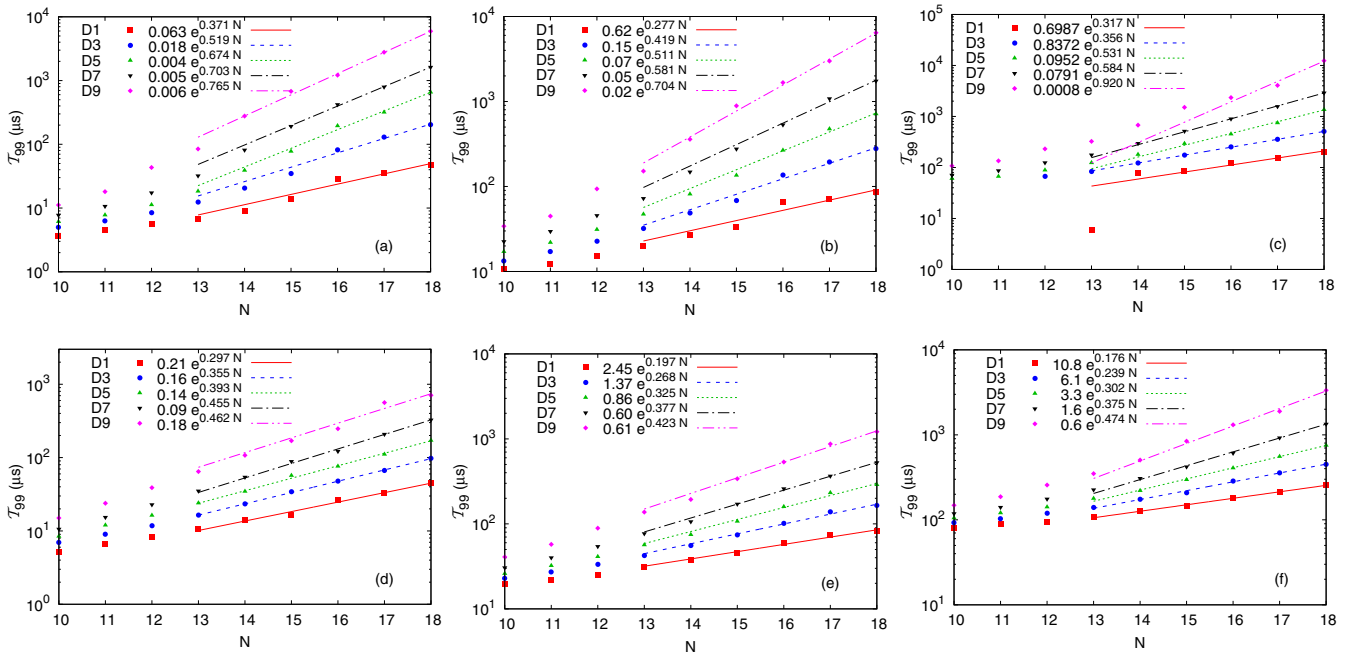

FIG. 12. Deciles for the $\mathcal{T}_{99}$ for the cases with a native embedding on (a)–(c) DW2000Q and (d)–(f) DWAdv for (a) and (d) $T_A = 4$ μs, (b) and (e) $T_A = 20$ μs, and (c) and (f) $T_A = 100$ μs.

Another distinguishing factor shown by the scaling results from the D-Wave systems compared to the simulation results is that the scaling exponents $r_{\mathcal{T}_{99}}$ become approximately smaller as the annealing time is increased on both D-Wave systems. A probable explanation for such a behavior is a more significant effect of the noise present in the systems for longer annealing times, as the system is in the quasistatic limit [64]. Moreover, unlike the annealing schedule used in the simulations, the D-Wave annealers do not use linear functions for $A(s)$ and $B(s)$.

VI. CONCLUSION

The goal of this work was to assess the performance of quantum annealing in solving 13 sets of hard 2-SAT problems corresponding to different problem sizes, using both simulations and the D-Wave quantum annealers. In addition to the standard Hamiltonian used for quantum annealing, we studied the performance of the algorithm in introducing two variations to the standard Hamiltonian in our simulations, by adding the ferromagnetic or the antiferromagnetic trigger Hamiltonian. The performance of the algorithm is determined by studying the distributions and/or scalings of three observables: the minimum energy gap between the ground state and the first excited state of the Hamiltonian, the success probability, and the time to solution.

Focusing first on the distributions of the minimum energy gaps for the given problems, using the three quantum annealing Hamiltonians considered in this work, we found three distinct distributions for different Hamiltonians considered in this work. Interestingly, we also obtained three kinds of success probability distributions from the simulations as well as the D-Wave systems, depending on the chosen annealing Hamiltonian and/or the annealing parameters. The numerically obtained success probability distributions for the standard quantum annealing Hamiltonian and those obtained using DW2000Q were bimodal for all the chosen annealing times. On the other hand, simulations using the annealing Hamiltonians with the ferromagnetic trigger Hamiltonian resulted in unimodal distributions for all the annealing times. Constant and bimodal success probability distributions were obtained numerically for the annealing Hamiltonian with the antiferromagnetic trigger Hamiltonian for different annealing times. Constant and unimodal distributions were also obtained from DWAdv, suggesting that slightly different mechanisms were at play in the two D-Wave systems.

Second, we found an exponential scaling of the minimum energy gaps for all the considered quantum annealing Hamiltonians (see Table I), confirming the hardness of the 2-SAT problems. As a consequence, the scaling of $\mathcal{T}_{99}$ in the case of an ideal adiabatic evolution using the standard quantum annealing Hamiltonian is worse than even a brute-force search of the ground state for the given problems. However for the short annealing time $T_A = 10$, the scaling exponent is significantly smaller. A similar trend was also observed upon adding the two trigger Hamiltonians. Such short annealing times lead to a diabatic evolution of the state of the system, which improves the scaling performance for the 2-SAT problems.

With the addition of the ferromagnetic and the antiferromagnetic trigger Hamiltonians to the annealing Hamiltonian, we observed a better scaling of the minimum energy gaps as a function of the problem size, especially for the former. This improvement also manifested as a smaller scaling exponent for the median $\mathcal{T}_{99}$ in both these cases and for the three annealing times compared to the standard quantum annealing Hamiltonian. Therefore, in the long annealing time regime, the addition of the ferromagnetic trigger Hamiltonian leads to the smallest scaling exponent for the median $\mathcal{T}_{99}$. On the other hand, since the addition of the antiferromagnetic trigger Hamiltonian facilitates various nonadiabatic mechanisms [52], for the given set of 2-SAT problems and short annealing time $T_A = 10$, we obtain the best scaling with the addition of the antiferromagnetic trigger Hamiltonian. The scaling exponent in this case is better also compared to that obtained using simulated annealing to solve these problems ($r_{\mathrm{SA}} = 0.34$) [43].

Although the chosen annealing times for the D-Wave devices are much longer than those for the simulations, the scaling behavior of the $\mathcal{T}_{99}$ obtained using DW2000Q is comparable to that of the short annealing time scaling of the standard quantum annealing Hamiltonian for all the considered annealing times (see Table II). This observation suggests that the D-Wave systems are not working ideally, and noise and temperature effects play a role similar to the nonadiabatic mechanisms in the case of simulations, in enhancing their scaling performance in solving the given set of problems. Furthermore, the scaling exponents for the median $\mathcal{T}_{99}$ obtained from DWAdv are even smaller, making the differences between the two systems evident. A better understanding of the temperature and noise effects in these systems calls for further investigation.

Although from our results it is noted that short annealing times in the case of simulations, and temperature and noise effects in the D-Wave systems are beneficial for the scaling complexity of quantum annealing, it should be emphasized that these observations are specific to hard 2-SAT problems.

TABLE I. Median scaling exponents r_Δ and $r_{\mathcal{T}_{99}}$ for minimum energy gaps and $\mathcal{T}_{99}$ for $T_A = 10, 100, 1000$, respectively, obtained from simulations for the three quantum annealing Hamiltonians. The scaling exponents for the theoretical runtimes are $r_{\mathrm{TR}} = 2|r_\Delta|$.

		$r_{\mathcal{T}_{99}}$		
Hamiltonian	r_Δ	$T_A = 10$	$T_A = 100$	$T_A = 1000$
standard	−0.529	0.530	1.170	1.205
ferromagnetic trigger	−0.212	0.373	0.475	0.478
antiferromagnetic trigger	−0.265	0.277	0.651	0.617

TABLE II. Median scaling exponent $r_{\mathcal{T}_{99}}$ for $T_A = 4, 20, 100$ μs, obtained by using DW2000Q and DWAdv.

	$r_{\mathcal{T}_{99}}$		
Device	$T_A = 4$ μs	$T_A = 20$ μs	$T_A = 100$ μs
DW2000Q	0.674	0.511	0.531
DWAdv	0.393	0.325	0.302

It is possible to obtain a different scaling behavior for other problems.

ACKNOWLEDGMENTS

The authors gratefully acknowledge the Gauss Centre for Supercomputing e.V. for funding this project by providing computing time through the John von Neumann Institute for Computing on the GCS Supercomputer JUWELS [66] at Jülich Supercomputing Centre. The authors also gratefully acknowledge the computing time granted through JARA on the supercomputer JURECA [67] at Forschungszentrum Jülich. V.M. acknowledges support from the project JUNIQ, which has received funding from the German Federal Ministry of Education and Research and the Ministry of Culture and Science of the State of North Rhine-Westphalia.

APPENDIX A: DISTRIBUTIONS

We present the probability distribution functions used in this work to fit the distributions of the minimum energy gap or its inverse, the correlation length. The first such distribution is the Fréchet distribution

$$F_k(x) = a\left(\frac{b}{x}\right)^{k+1} e^{-(b/x)^k}, \tag{A1}$$

where a, b, and k are constants. The second is the Weibull distribution, which is given by

$$W_k(x) = a\left(\frac{x}{b}\right)^{k-1} e^{-(x/b)^k}. \tag{A2}$$

We also define the translated Weibull distribution

$$W_k(x) = a\left(\frac{x-\mu}{b}\right)^{k-1} e^{-[(x-\mu)/b]^k}, \tag{A3}$$

where μ is the extent of the translation. Finally, we derive the distribution for a variable $y = 1/x$, if the distribution for x is found to follow the translated Weibull distribution. The Jacobian for this mapping is $J = \|\partial x/\partial y\| = 1/x^2$ and therefore

$$W_k(y) = a(1-\mu y)^2\left(\frac{1-\mu y}{by}\right)^{k+1} e^{-[(1-\mu y)/b\Delta_{\min}]^k}. \tag{A4}$$

This distribution will be referred to as the transformed, translated Weibull distribution.

APPENDIX B: MAPPING SUCCESS PROBABILITY DISTRIBUTIONS FROM THE DISTRIBUTIONS OF THE MINIMUM ENERGY GAP

From a theoretical perspective, the Landau-Zener theory can provide a mapping between the minimum energy gap and the success probability [43] if the annealing time is long enough to allow for an adiabatic evolution of the system. According to the formula

$$p = 1 - e^{-\gamma \Delta_{\min}^2}, \tag{B1}$$

the parameter γ controls the speed of the sweep, which in turn is controlled by the annealing time. Thus,

$$\Delta_{\min} = \gamma^{-1/2}\{-\ln(1-p)\}^{1/2}, \tag{B2}$$

and the Jacobian is given by

$$\|\partial \Delta_{\min}/\partial p\| = \frac{1}{2}\gamma^{-1}\frac{1}{\Delta_{\min}} e^{\gamma \Delta_{\min}^2}. \tag{B3}$$

Hence, if the probability distribution function for the minimum energy gaps $\mathcal{P}(\Delta_{\min})$ is known, it is possible to obtain the success probability distribution

$$\mathcal{P}(p)dp = C^{-1}\mathcal{P}(\Delta_{\min})\gamma^{-1}\frac{1}{\Delta_{\min}} e^{\gamma \Delta_{\min}^2} dp, \tag{B4}$$

up to the normalization constant C^{-1} [43].

If we find the minimum energy gap distribution to follow the Weibull distribution function with $k = 2$, i.e.,

$$\mathcal{P}(\Delta_{\min}) = a\left(\frac{\Delta_{\min}}{b}\right) e^{-(\Delta_{\min}/b)^2}, \tag{B5}$$

for a certain parameter b and the normalization constant a, then substituting $\mathcal{P}(\Delta_{\min})$ in Eq. (B4) and setting the parameter $\gamma = 1/b^2$, we obtain $\mathcal{P}(P_{\text{succ}})dP_{\text{succ}} = \mathcal{P}(p|_{\gamma=1/b^2})\,dP_{\text{succ}}$ to be constant. Similarly, it is possible to obtain unimodal or bimodal distributions for the success probability distribution $\mathcal{P}(P_{\text{succ}})$ if we tune the annealing time by means of γ to the point where $\langle P_{\text{succ}}\rangle = 1/2$, depending on the distribution functions that the minimum energy gaps follow.

[1] S. Kirkpatrick, D. Gelatt, and M. P. Vecchi, Optimization by simulated annealing, Science **220**, 671 (1983).

[2] B. Apolloni, N. Cesa-Bianchi, and D. De Falco, in *Proceedings of the International Conference on Stochastic Processes, Physics and Geometry, Ascona/Locarno, 1988*, edited by S. Albeverio, G. Casati, U. Cattaneo, D. Merlini, and R. Moresi, Vol. 97 (World Scientific, Singapore, 1988).

[3] A. B. Finnila, M. A. Gomez, C. Sebenik, C. Stenson, and J. D. Doll, Quantum annealing: A new method for minimizing multidimensional functions, Chem. Phys. Lett. **219**, 343 (1994).

[4] T. Kadowaki and H. Nishimori, Quantum annealing in the transverse Ising model, Phys. Rev. E **58**, 5355 (1998).

[5] E. Farhi, J. Goldstone, S. Gutmann, and M. Sipser, Quantum computation by adiabatic evolution, arXiv:quant-ph/0001106.

[6] E. Farhi, J. Goldstone, S. Gutmann, J. Lapan, A. Lundgren, and D. Preda, A quantum adiabatic evolution algorithm applied to random instances of an NP-complete problem, Science **292**, 472 (2001).

[7] E. Crosson, E. Farhi, C. Y.-Y. Lin, Cedric, H.-H. Lin, and P. Shor, Different strategies for optimization using the quantum adiabatic algorithm, arXiv:1401.7320.

[8] S. Muthukrishnan, T. Albash, and D. A. Lidar, Tunneling and Speedup in Quantum Optimization for Permutation-Symmetric Problems, Phys. Rev. X **6**, 031010 (2016).

[9] L. Hormozi, E. W. Brown, G. Carleo, and M. Troyer, Nonstoquastic Hamiltonians and quantum annealing of an Ising spin glass, Phys. Rev. B **95**, 184416 (2017).

[10] E. Farhi, J. Goldstone, and S. Gutmann, A quantum approximate optimization algorithm, arXiv:1411.4028.

[11] E. Farhi and A. W. Harrow, Quantum supremacy through the quantum approximate optimization algorithm, arXiv:1602.07674.

[12] L. Zhou, S.-T. Wang, S. Choi, H. Pichler, and M. D. Lukin, Quantum Approximate Optimization Algorithm: Performance, Mechanism, and Implementation on Near-Term Devices, Phys. Rev. X **10**, 021067 (2020).

[13] S. Hadfield, Z. Wang, B. O'Gorman, E. G. Rieffel, D. Venturelli, and R. Biswas, From the quantum approximate optimization algorithm to a quantum alternating operator ansatz, Algorithms **12**, 34 (2019).

[14] M. Willsch, D. Willsch, F. Jin, H. De Raedt, and K. Michielsen, Benchmarking the quantum approximate optimization algorithm, Quantum Inf. Process. **19**, 197 (2020).

[15] J. Brooke, D. Bitko, T. F. Rosenbaum, and G. Aeppli, Quantum annealing of a disordered magnet, Science **284**, 779 (1999).

[16] G. E. Santoro, R. Martoňák, E. Tosatti, and R. Car, Theory of quantum annealing of an Ising spin glass, Science **295**, 2427 (2002).

[17] R. Martoňák, G. E. Santoro, and E. Tosatti, Quantum annealing of the traveling-salesman problem, Phys. Rev. E **70**, 057701 (2004).

[18] G. E. Santoro and E. Tosatti, Optimization using quantum mechanics: Quantum annealing through adiabatic evolution, J. Phys. A: Math. Gen. **41**, 209801 (2008).

[19] Y. Seki and H. Nishimori, Quantum annealing with antiferromagnetic fluctuations, Phys. Rev. E **85**, 051112 (2012).

[20] R. D. Somma, D. Nagaj, and M. Kieferová, Quantum Speedup by Quantum Annealing, Phys. Rev. Lett. **109**, 050501 (2012).

[21] Y. Susa, Y. Yamashiro, M. Yamamoto, and H. Nishimori, Exponential speedup of quantum annealing by inhomogeneous driving of the transverse field, J. Phys. Soc. Jpn. **87**, 023002 (2018).

[22] T. Albash and D. A. Lidar, Adiabatic quantum computation, Rev. Mod. Phys. **90**, 015002 (2018).

[23] T. Hsu, F. Jin, C. Seidel, F. Neukart, H. De Raedt, and K. Michielsen, Quantum annealing with anneal path control: Application to 2-SAT problems with known energy landscapes, Commun. Comput. Phys. **26**, 928 (2019).

[24] P. Hauke, H. G. Katzgraber, W. Lechner, H. Nishimori, and W. D. Oliver, Perspectives of quantum annealing: Methods and implementations, Rep. Prog. Phys. **83**, 054401 (2020).

[25] E. J. Crosson and D. A. Lidar, Prospects for quantum enhancement with diabatic quantum annealing, Nat. Rev. Phys. **3**, 466 (2021).

[26] C. McGeoch and P. Farré, The D-Wave Advantage system: An overview, D-Wave Systems Inc. Report No. 14-1049A-A, 2020 (unpublished).

[27] M. W. Johnson, M. H. S. Amin, S. Gildert, T. Lanting, F. Hamze, N. Dickson, R. Harris, A. J. Berkley, J. Johansson, P. Bunyk, E. M. Chapple, C. Enderud, J. P. Hilton, K. Karimi, E. Ladizinsky, N. Ladizinsky, T. Oh, I. Perminov, C. Rich, M. C. Thom *et al.*, Quantum annealing with manufactured spins, Nature (London) **473**, 194 (2011).

[28] N. G. Dickson, M. W. Johnson, M. H. Amin, R. Harris, F. Altomare, A. J. Berkley, P. Bunyk, J. Cai, E. M. Chapple, P. Chavez, F. Cioata, T. Cirip, P. deBuen, M. Drew-Brook, C. Enderud, S. Gildert, F. Hamze, J. P. Hilton, E. Hoskinson, K. Karimi *et al.*, Thermally assisted quantum annealing of a 16-qubit problem, Nat. Commun. **4**, 1903 (2013).

[29] K. L. Pudenz, T. Albash, and D. A. Lidar, Error-corrected quantum annealing with hundreds of qubits, Nat. Commun. **5**, 3243 (2014).

[30] T. Lanting, A. J. Przybysz, A. Y. Smirnov, F. M. Spedalieri, M. H. Amin, A. J. Berkley, R. Harris, F. Altomare, S. Boixo, P. Bunyk, N. Dickson, C. Enderud, J. P. Hilton, E. Hoskinson, M. W. Johnson, E. Ladizinsky, N. Ladizinsky, R. Neufeld, T. Oh, I. Perminov *et al.*, Entanglement in a Quantum Annealing Processor, Phys. Rev. X **4**, 021041 (2014).

[31] S. Boixo, T. F. Rønnow, S. V. Isakov, Z. Wang, D. Wecker, D. A. Lidar, J. M. Martinis, and M. Troyer, Evidence for quantum annealing with more than one hundred qubits, Nat. Phys. **10**, 218 (2014).

[32] S. Boixo, V. N. Smelyanskiy, A. Shabani, S. V. Isakov, M. Dykman, V. S. Denchev, M. H. Amin, A. Y. Smirnov, M. Mohseni, and H. Neven, Computational multiqubit tunnelling in programmable quantum annealers, Nat. Commun. **7**, 10327 (2016).

[33] T. Albash and D. A. Lidar, Demonstration of a Scaling Advantage for a Quantum Annealer over Simulated Annealing, Phys. Rev. X **8**, 031016 (2018).

[34] S. Okada, M. Ohzeki, M. Terabe, and S. Taguchi, Improving solutions by embedding larger subproblems in a D-Wave quantum annealer, Sci. Rep. **9**, 2098 (2019).

[35] A. Pearson, A. Mishra, I. Hen, and D. Lidar, Analog errors in quantum annealing: Doom and hope, npj Quantum Inf. **5**, 107 (2019).

[36] R. Ayanzadeh, M. Halem, and T. Finin, Quantum annealing: A hybrid quantum learning automata, Sci. Rep. **10**, 7952 (2020).

[37] P. Weinberg, M. Tylutki, J. M. Rönkkö, J. Westerholm, J. A. Åström, P. Manninen, P. Törmä, and A. W. Sandvik, Scaling and Diabatic Effects in Quantum Annealing with a D-Wave Device, Phys. Rev. Lett. **124**, 090502 (2020).

[38] E. Grant, T. S. Humble, and B. Stump, Benchmarking Quantum Annealing Controls with Portfolio Optimization, Phys. Rev. Applied **15**, 014012 (2021).

[39] C. D. G. Calaza, D. Willsch, and K. Michielsen, Garden optimization problems for benchmarking quantum annealers, Quantum Inf. Process. **20**, 1 (2021).

[40] T. F. Rønnow, Z. Wang, J. Job, S. Boixo, S. V. Isakov, D. Wecker, J. M. Martinis, D. A. Lidar, and M. Troyer, Defining and detecting quantum speedup, Science **345**, 420 (2014).

[41] J. King, S. Yarkoni, M. M. Nevisi, J. P. Hilton, and C. C. McGeoch, Benchmarking a quantum annealing processor with the time-to-target metric, arXiv:1508.05087.

[42] I. Hen, J. Job, T. Albash, T. F. Rønnow, M. Troyer, and D. A. Lidar, Probing for quantum speedup in spin-glass problems with planted solutions, Phys. Rev. A **92**, 042325 (2015).

[43] T. Neuhaus, Quantum searches in a hard 2SAT ensemble, arXiv:1412.5460.

[44] D. Willsch, M. Willsch, F. Jin, K. Michielsen, and H. De Raedt, GPU-accelerated simulations of quantum annealing and the quantum approximate optimization algorithm, Comput. Phys. Commun. **278**, 108411 (2022).

[45] M. S. Könz, W. Lechner, H. G. Katzgraber, and M. Troyer, Scaling overhead of embedding optimization problems in quantum annealing, PRX Quantum **2**, 040322 (2021).

[46] T. Neuhaus, Monte Carlo search for very hard KSAT realizations for use in quantum annealing, arXiv:1412.5361.

[47] M. H. S. Amin, Consistency of the Adiabatic Theorem, Phys. Rev. Lett. **102**, 220401 (2009).

[48] E. Farhi, J. Goldstone, and S. Gutmann, Quantum adiabatic evolution algorithms with different paths, arXiv:quant-ph/0208135.

[49] L. Zeng, J. Zhang, and M. Sarovar, Schedule path optimization for adiabatic quantum computing and optimization, J. Phys. A: Math. Theor. **49**, 165305 (2016).

[50] A. B. Özgüler, R. Joynt, and M. G. Vavilov, Steering random spin systems to speed up the quantum adiabatic algorithm, Phys. Rev. A **98**, 062311 (2018).

[51] E. M. Lykiardopoulou, A. Zucca, S. A. Scivier, and M. H. Amin, Improving nonstoquastic quantum annealing with spin-reversal transformations, Phys. Rev. A **104**, 012619 (2021).

[52] V. Mehta, F. Jin, H. De Raedt, and K. Michielsen, Quantum annealing with trigger Hamiltonians: Application to 2-satisfiability and nonstoquastic problems, Phys. Rev. A **104**, 032421 (2021).

[53] M. Born and V. Fock, Beweis des adiabatensatzes, Z. Phys. **51**, 165 (1928).

[54] T. Kato, On the adiabatic theorem of quantum mechanics, J. Phys. Soc. Jpn. **5**, 435 (1950).

[55] S. Jansen, M.-B. Ruskai, and R. Seiler, Bounds for the adiabatic approximation with applications to quantum computation, J. Math. Phys. **48**, 102111 (2007).

[56] L. D. Landau, Zur theorie der energieubertragung I, Phys. Z. Sowjetunion **1**, 88 (1932).

[57] C. Zener, Non-adiabatic crossing of energy levels, Proc. R. Soc. London Ser. A **137**, 696 (1932).

[58] H. De Raedt, S. Miyashita, K. Saito, D. García-Pablos, and N. García, Theory of quantum tunneling of the magnetization in magnetic particles, Phys. Rev. B **56**, 11761 (1997).

[59] J. K. Cullum and R. A. Willoughby, *Lanczos Algorithms for Large Symmetric Eigenvalue Computations* (SIAM, Philadelphia, 2002), Vol. I.

[60] M. Suzuki, S. Miyashita, and A. Kuroda, Monte Carlo simulation of quantum spin systems. I, Prog. Theor. Phys. **58**, 1377 (1977).

[61] H. De Raedt, Product formula algorithms for solving the time dependent Schrödinger equation, Comput. Phys. Rep. **7**, 1 (1987).

[62] J. Huyghebaert and H. De Raedt, Product formula methods for time-dependent Schrödinger problems, J. Phys. A: Math. Gen. **23**, 5777 (1990).

[63] N. Hatano and M. Suzuki, in *Quantum Annealing and Other Optimization Methods*, edited by A. Das and B. Chakrabarti, Lecture Notes in Physics, Vol. 679 (Springer, Berlin, 2005), pp. 37–68.

[64] M. H. Amin, Searching for quantum speedup in quasistatic quantum annealers, Phys. Rev. A **92**, 052323 (2015).

[65] M. Willsch, D. Willsch, F. Jin, H. De Raedt, and K. Michielsen, Real-time simulation of flux qubits used for quantum annealing, Phys. Rev. A **101**, 012327 (2020).

[66] D. Krause, JUWELS: Modular Tier-0/1 supercomputer at the Jülich Supercomputing Centre, J. Large-Scale Res. Fac. **5**, A135 (2019).

[67] D. Krause and P. Thörnig, JURECA: Modular supercomputer at Jülich Supercomputing Centre, J. Large-Scale Res. Fac. **4**, A132 (2018).